

Document downloaded from:

<http://hdl.handle.net/10251/170956>

This paper must be cited as:

Sabate-Fornons, F.; Jorda Moret, J.L.; Sabater Picot, M.J.; Corma Canós, A. (2020).  
Synthesis of isomorphically substituted Ru manganese molecular sieves and their catalytic  
properties for selective alcohol oxidation. *Journal of Materials Chemistry A*. 8(7):3771-3784.  
<https://doi.org/10.1039/c9ta11903e>



The final publication is available at  
<https://doi.org/10.1039/c9ta11903e>

Copyright The Royal Society of Chemistry

Additional Information

**Synthesis of isomorphically substituted Ru manganese molecular sieves and their catalytic properties for selective alcohol oxidation**

Ferran Sabaté, José L. Jordá, María J. Sabater\*, Avelino Corma\*

*Instituto de Tecnología Química, Universitat Politècnica de València - Consejo Superior de Investigaciones Científicas, Avenida Los Naranjos s/n, 46022, València, (Spain); \* e-mail: M.J.S: [mjsabate@itq.upv.es](mailto:mjsabate@itq.upv.es); A.C: [acorma@itq.upv.es](mailto:acorma@itq.upv.es)*

## **Abstract**

Ruthenium has been incorporated into the framework of the cryptomelane type manganese oxide K-OMS-2 ([Ru]-K-OMS2) and the presence of this element into the structure has been assessed by combining analytical and vibrational techniques such as ICP, UV-Vis, FT-IR and Raman spectroscopies, X-ray diffraction, electron microscopy (HR-TEM and SEM), TPR-H<sub>2</sub>, and X-ray photoelectron spectroscopy. Rietveld refinement of the X-ray diffractogram has allowed to estimate changes in the values of cell parameters which were compatible with an isomorphic ruthenium substitution into the original structure. These calculations are in agreement with the observed increase in the interplanar spacing of (100) planes from 7.1Å to 7.7Å for the Ru-doped material.

The consequence of the isomorphic substitution of Ru is the weakening of the Mn-O link, a fact that has important implications in catalysis, especially for those reactions that follow a Mars van-Krevelen type oxidation mechanism as can be the oxidation of alcohols to aldehydes. In this context, the results obtained display that [Ru]-K-OMS2 becomes a more active catalyst giving an excellent selectivity towards the aldehyde during the oxidation of alcohols, and a clear improvement of the catalytic properties with respect the undoped K-OMS2. The process is catalytically heterogeneous and the catalyst has been recovered and reused without a significant loss of activity and catalytic properties.

## Introduction

Mn-based oxides are promising materials for technological applications such as electrode materials (batteries), chemical sensing, separations and catalysis, mainly due to its high redox potential, environmental friendliness and low cost [1-9]

Manganese oxides can exist as a variety of stable oxides (*i.e.* MnO, Mn<sub>3</sub>O<sub>4</sub>, Mn<sub>2</sub>O<sub>3</sub>, MnO<sub>2</sub>, etc, ...) with different crystal structures, morphologies, porosities and textures that have been associated with a variety of properties. From this it follows that the variation of structural and chemical parameters can be the key for modulating their catalytic activity [10, 11].

K-OMS2 is a crystalline microporous Mn-based oxide with a high void volume (4.6Å x 4.6Å x 4.6Å); and a chemical composition of KMn<sub>8</sub>O<sub>16</sub> consisting of VIII-coordinated tunnel sites bound by four Mn<sub>2</sub>O<sub>6</sub><sup>4-</sup> sheets 90° to each other (see Figure S1 taken from ref 12, Supporting Information). K-OMS2 has a mixed valence manganese framework due to the coexistence of Mn<sup>4+</sup> and Mn<sup>3+</sup> ions (and sometimes even Mn<sup>2+</sup>), that causes the network to have a negative charge that needs to be compensated by interstitial K<sup>+</sup> ions (see Figure S1, Supporting Information). Due to this particular chemical composition and stability of the three-dimensional structure, attention has been paid to modify its crystalline system, particle size and morphology in an effort to modify its original physico-chemical properties and improve its performance as a catalyst [10].

The properties of cryptomelane-type material K-OMS-2 have also been modified by replacing a fraction of the structural Mn cations by other ions (*i.e.* Co, Fe, Zn, Mo, etc...)[10]. In this context we have undertaken the substitution of manganese by ruthenium in the manganese molecular sieve of cryptomelane-type K-OMS-2 to get a structural analog [Ru]-K-OMS2, based on a combination of both elements, *i.e.* Mn and Ru. The most striking effect of doping with Ru is the weakening of the Mn-O bond so that oxygen atoms can be more easily removed from the surface layer; a fact that theoretically facilitates the production of oxygen vacancy defects (OVDs), which are key for certain catalytic applications. [13]

Since OVDs are in principle good descriptors for the ability of oxides to participate in oxidation reactions, and given that the synthesis of aldehydes and ketones from alcohols are relevant industrially [14], we have used the oxidation of alcohols to aldehydes as a model reaction to study the changes in the structural and physico-chemical properties of this material and their influence on the catalytic activity due to doping with Ru. Indeed, the incorporation of Ru should favor the oxygen uptake and possibly given by the

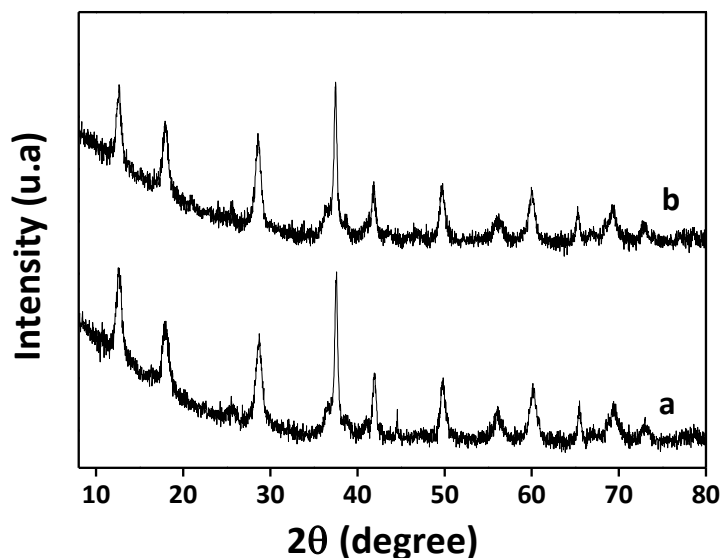
structure will enhance chemical oxidation occurring through a Mars –van Krevelen mechanism of the mixed oxide. [10, 15-19]

## Results and Discussion

Following previous reports on the synthesis of isomorphic substituted cryptomelane-type materials, the synthesis of [Ru]-K-OMS2 was accomplished by a template/surfactant-free reaction between  $\text{KMnO}_4$  and  $\text{MnSO}_4$ , to which  $\text{RuCl}_3$  (2% by weight Ru) was incorporated drop-wise as the source of Ru dopant cation (see Experimental Section) [10]. The resulting [Ru]-K-OMS2 (2 wt%) was characterized looking for possible similarities and differences with the original un-doped K-OMS2 material (see Experimental Section) by means of different techniques.

### X-Ray diffraction and morphological characterization

X-Ray diffraction (XRD) was used to confirm the identity of the Ru-doped solid. In this case the XRD patterns were in good agreement with those previously reported for cryptomelane-type materials, hence confirming that this was the crystallized phase (Figure 1). [20]



**Figure 1:** XRD patterns of undoped material K-OMS2 (a) and doped material [Ru]- K-OMS2 (2 wt%) (b).

It is important to indicate that the absence of additional peaks in the diffractogram of [Ru]-K-OMS2 (2 wt%) led us to rule out the formation of any manganese and/or ruthenium segregated samples, hence suggesting that the Ru-doped cryptomelane crystallizes as a pure phase (Figure 1).

Interestingly, when the cell parameters of both materials, i.e. K-OMS2 and [Ru]-K-OMS2 (2 wt%) were refined with the program FullProf [21] using the  $I4/m$  space group, the calculated values for the non-doped material were  $a=b= 9.8345\text{\AA}$  and  $c = 2.8523\text{\AA}$ , while the cell parameters for the Ru-doped material were  $a=b= 9.8401\text{\AA}$  and  $c = 2.8552\text{\AA}$ . From these results a small expansion of the unit cell could be deduced for the new Ru-doped oxide, which was attributed to the substitution of Mn for the slightly larger Ru atoms [22].

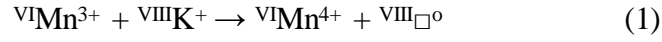
This fact is in accordance with chemical analysis data obtained by IPC which showed that the amount of  $\text{K}^+$  remained unchanged, while the amount of  $\text{Mn}^{n+}$  was appreciably reduced (Table 1) in the Ru-doped sample. From these results we inferred that the replacement of a manganese fraction by ruthenium may have taken place after the doping process in the new cryptomelane structure [Ru]-K-OMS2 (2 wt%), so that ruthenium would preferably replace manganese atoms located in the framework rather than the potassium cations located in the tunnels [10, 23, 24]. Indeed theoretically when ruthenium is incorporated into the structure, an octahedral ruthenium ion ( $^{\text{VI}}\text{Ru}^{3+}$ ) should displace an octahedral manganese ion ( $^{\text{VI}}\text{Mn}^{3+}$ ) without generating a vacancy and the electroneutrality of the system should be kept, hence giving rise to a very stable structure.

**Table 1** Chemical composition of K-OMS2 and [Ru]-K-OMS2 (2 wt%) obtained by ICP-AES.

Entry	Sample	Element (wt%)				K/Mn (molar ratio)	Ru/Mn (molar ratio)
		Mn	K	Ru	K / Mn		
1	K-OMS2	61.4	4.9	-	0.08	0.112	-
2	[Ru]-K-OMS2 (2wt%)	55.6	4.8	2.0	0.09	0.122	0.02

Moreover, given the similarity between the ion radii of  $\text{Ru}^{3+}$  and  $\text{Mn}^{3+}$ , the isomorphous substitution, if occurred, should more likely occur at  $\text{Mn}^{3+}$  positions and not at the tetravalent  $\text{Mn}^{4+}$  ones [25, 26].

According to the chemical composition obtained experimentally, the empirical formula for the un-doped material should be  $K_{0.112}MnO_2$  thus fitting with the redox exchange proposed by Feng *et al.* [27] that gives the general formula  $K_xMn^{4+}_{1-x}Mn^{3+}_xO_2$ , through the equation (1):



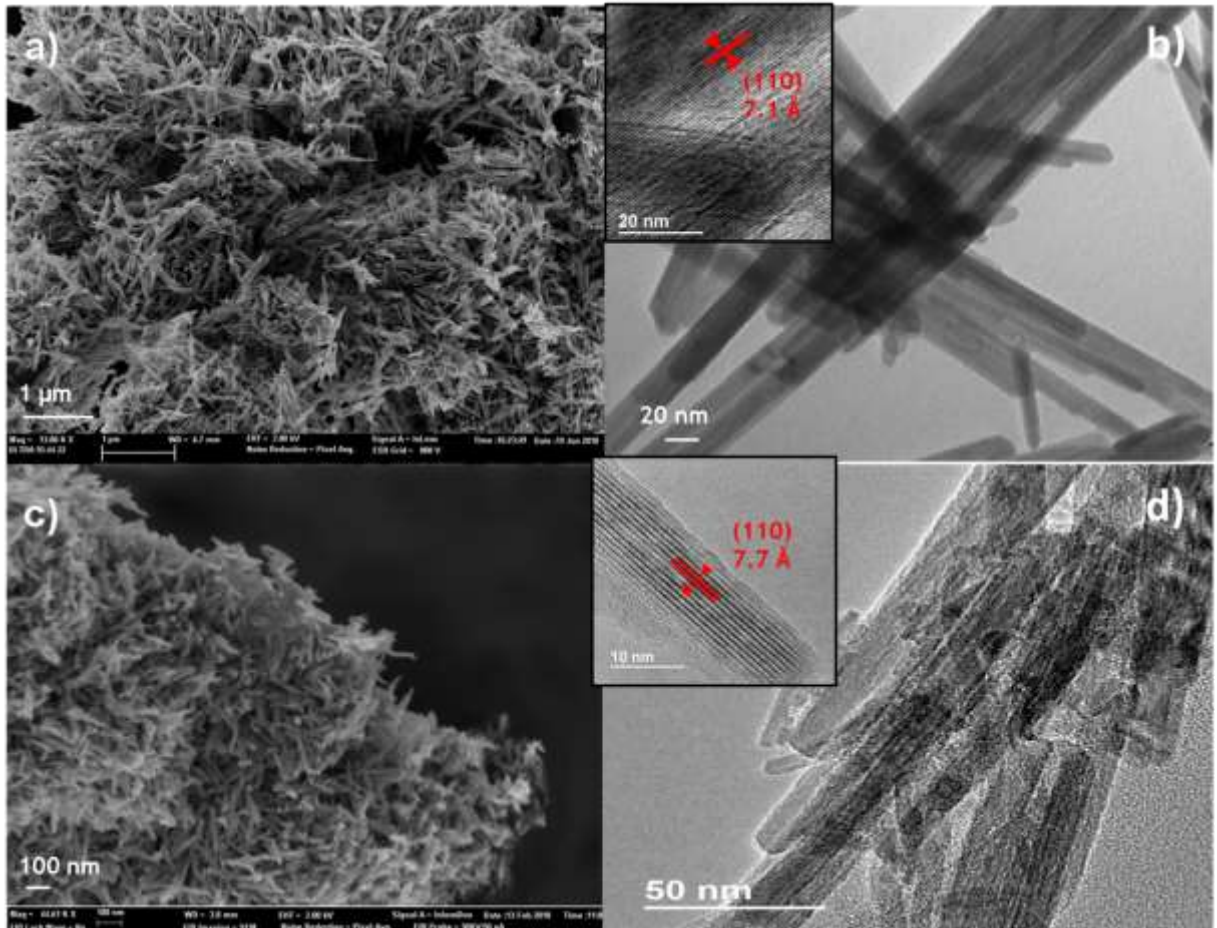
where  ${}^{VIII}\square^o$  is a vacant tunnel site and the super index (*i.e.* VI, VIII) indicates the lattice and the tunnel positions respectively. In this case, the general formula is  $K_{0.112}Mn^{4+}_{0.888}Mn^{3+}_{0.112}O_2$  and the average oxidation state (AOS)[28] is 3.89.

Following with this reasoning and according to ICP analysis (Table 1), if we assume that octahedral  ${}^{VI}Ru^{3+}$  ions are replacing  ${}^{VI}Mn^{3+}$  without generating a vacancy, then the general formula for this statement could be expressed as  $K_xMn^{4+}_{1-x}Mn^{3+}_{x-y}Ru^{3+}_yO_2$  giving the empirical formula  $K_{0.09}Mn^{4+}_{0.91}Mn^{3+}_{0.07}Ru^{3+}_{0.02}O_2$ , therefore giving values that can enter into the range of the structural limitations of the cryptomelane described in the literature [28]. In this case, the average oxidation state (AOS) calculated for the Ru-doped sample was 3.91.

Besides, in order to study the influence of Ru-doping on the surface area of the catalyst, the latter was measured using  $CO_2$  isotherms at 273K [29] (Supporting Information, Table S2) and we obtained that the surface area increased from 52.2 to 131.1  $m^2.g^{-1}$  for the original K-OMS2 and [Ru]-K-OMS2 (2 wt%) respectively [10, 30].

### Scanning and Transmission Electron Microscopies

The global morphology of both materials K-OMS2 and [Ru]-K-OMS2 (2 wt%) was examined and compared by scanning electron and transmission electron microscopies (SEM and HR-TEM). Figure 2 includes different SEM micrographs of both crystalline structures, showing that K-OMS-2 and [Ru]-K-OMS2 (2 wt%) had similar needlelike shape (or nanorods), which is typical for cryptomelane-type materials, a fact that reinforces the aforementioned hypothesis on the structural integrity of [Ru]-K-OMS2 (2 wt%) (Figure 2).



**Figure 2.** SEM and HR-TEM micrographs of undoped and [Ru]-doped cryptomelane [Ru]-K-OMS2 (2 wt%): a) SEM micrograph of K-OMS2, b) HR-TEM micrograph of K-OMS2, c) SEM micrograph of [Ru]-K-OMS2 (2 wt%) and d) HR-TEM micrograph of [Ru]-K-OMS2 (2 wt%). The insets show HR-TEM images of original K-OMS2 and [Ru]-K-OMS2(2 wt%) showing the interplanar spacing.

HR-TEM micrographs were also used to estimate the dimensions of the Ru containing nanorods, which were about 130-500 nm [10, 22]. Along with this and according to the unit cell expansion previously observed in section X-Ray Diffraction and Morphology, the interplanar spacing of (110) planes also increased from 7.1Å to 7.7Å for the Ru-doped material in accordance with previous results in the literature for other isomorphic substitutions (Figure 2) [10, 22]

The elemental mapping by means of high-angle annular dark-field scanning transmission electron microscopy (HAADF-STEM) with energy-dispersive X ray (EDX) as well as XEDS-SEM clearly showed the existence of a homogeneous distribution of Ru along the entire crystal, a fact that we interpret as due to a regular



incorporation of Ru in the framework (Figure S2, Supporting Information). The values obtained are similar to values obtained from ICP – AES analysis (Table S1, Supporting Information).

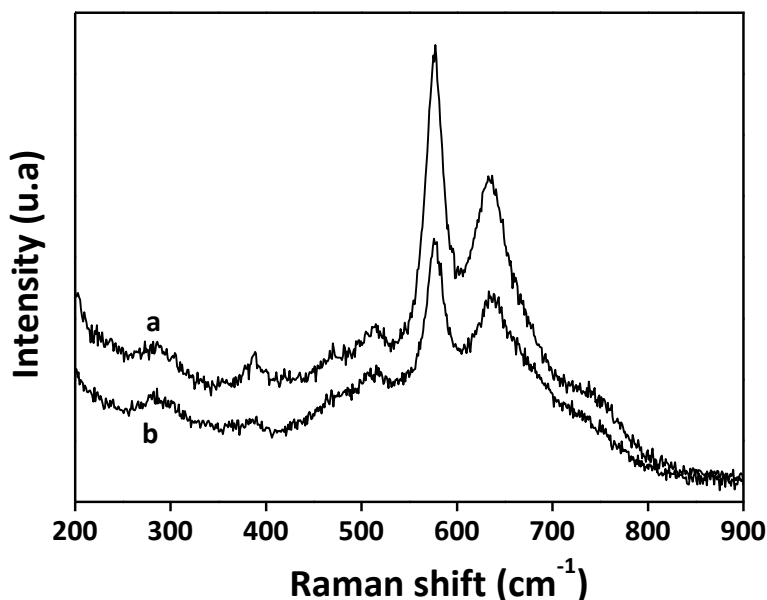
#### Thermal stability (TGA and DTG studies)

Thermogravimetric Analyses (TGA) and Derivative Thermogravimetry (DTG) studies of the thermal decomposition of un-doped and Ru-doped cryptomelane [Ru]-K-OMS2 (2 wt%) under nitrogen atmosphere showed that both samples follow the same behavior when increasing the temperature.

As shown in Figure S3 (Supporting Information) the DTG curves showed that both samples present two major weight losses [10, 29, 31, 32]: the first one, which takes place below 250°C and is accompanied by an endothermic peak, is assigned to desorption of physisorbed H<sub>2</sub>O and O<sub>2</sub> molecules from the surface [10, 33] The second one corresponds to a smooth and continuous weight loss detected up to about 600°C, which is related to an endothermic process which was attributed to desorption of chemisorbed H<sub>2</sub>O (inside the 2x2 tunnels) together with the evolution of structural oxygen near the surface (without decomposition of the material) [7]. Finally, the intense peak detected about 600°C, is associated to different crystalline phase transfer processes that involve endothermic events (Figure S3). For instance, the evolution of oxygen from the framework which results in a crystallographic transition to Mn<sub>2</sub>O<sub>3</sub> and Mn<sub>3</sub>O<sub>4</sub> according to literature references [23, 32, 34]. Then, the consequence that can be drawn from these studies is that the incorporation of Ru into the structure has no significant effects on the decomposition pattern of the original cryptomelane, at least at the relatively low levels of Ru presented here.

#### Raman and FT-IR spectroscopy

The Raman spectra of K-OMS2 and [Ru]-K-OMS2 (2 wt%) were very similar although in general the peaks of the Ru-doped material were less intense than the same peaks in the non-doped reference material K-OMS2 (Figure 3).



**Figure 3** Raman spectra of K-OMS2 a) and [Ru]-K-OMS2 (2 wt%) b)

As can be deduced from Figure 3, the Raman spectra of [Ru]-K-OMS2 (2 wt%) and K-OMS2 showed two intense peaks centered at 633 and 577  $\text{cm}^{-1}$ , which were assigned to  $A_{1g}$  and  $F_{2g}$  Mn-O lattice vibrational modes, together with a shoulder at 753  $\text{cm}^{-1}$  [33]. Other less intense peaks at 530, 480 and 386  $\text{cm}^{-1}$  characteristics of the original cryptomelane structure were also present in the Ru-doped material (Figure 3).

The two sharp bands at 577 and 636  $\text{cm}^{-1}$  were associated to two different Mn-O vibrations [33]: the band at 636  $\text{cm}^{-1}$  can be assigned to Mn-O vibrations that take place perpendicularly to the octahedron chains, whereas the band at 577  $\text{cm}^{-1}$  can be assigned to Mn-O vibrations along the octahedron framework. Finally the small band at 386  $\text{cm}^{-1}$  and the shoulder at 753  $\text{cm}^{-1}$  can be ascribed to the Mn-O bending vibrations and antisymmetric Mn-O stretching vibrations, respectively [33]. The absence of new bands associated to other manganese and/or ruthenium oxides led us to rule out the formation of segregated phases, a fact that could be taken as evidence of the purity of the Ru-doped material [35].

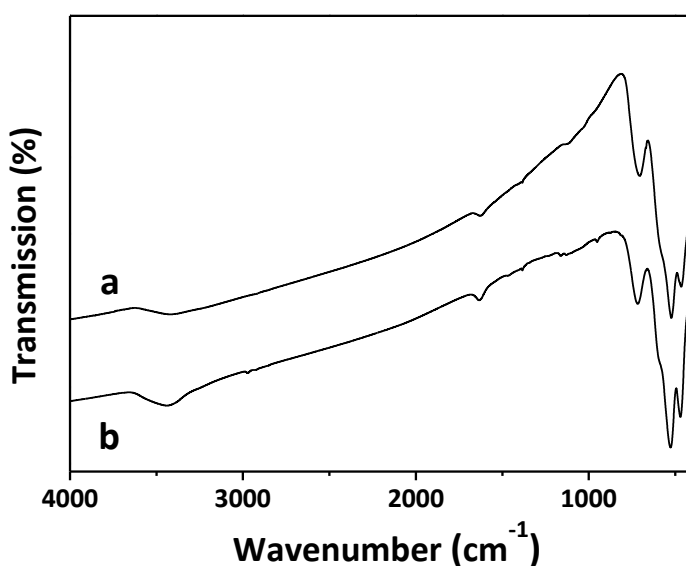
Thus, despite the absence of direct evidences about the location of the Ru in the framework, we made some attempts to know the plausible influence of Ru doping on the strength of the Mn-O bond, using an indirect way. For achieving this, and from a semiempirical point of view, the Mn-O force constant ( $k$ ) was calculated for both materials on the bases of the Hooke's Law according to the following expression [36] :

$$\tilde{\nu} = \frac{1}{2\pi c} \sqrt{\frac{k}{\mu}} \Rightarrow k = \mu \cdot (2\pi \cdot \tilde{\nu} \cdot c)^2$$

where  $\tilde{\nu}$  is the Raman shift ( $\text{cm}^{-1}$ ),  $c$  is light velocity and  $\mu$  is the effective mass.

Interestingly, by applying this equation we obtained that  $k_1(\text{Mn} - \text{O})$  in the original K-OMS-2 ( $k_1 = 308.564 \text{ N/m}$ ) was greater than the constant for the [Ru]-K-OMS2 (2 wt%) material ( $k_2 = 299.143 \text{ N/m}$ ). These results have important catalytic implications because they suggest that the Mn-O bond has weakened by effect of doping with Ru, a fact that *a priori* may have an impact on the catalytic applications as it will be shown later.

In line with previous Raman results, no new bands associated with structural Ru could be detected in the FT-IR spectrum of [Ru]-K-OMS2 (2 wt%) (Figure 4).



**Figure 4** FT-IR spectrum of K-OMS2 (a) and Ru-K-OMS2 (2 wt%) (b)

In this context, [Ru]-K-OMS2 (2 wt%) showed similar bands as K-OMS2 below  $1000 \text{ cm}^{-1}$  that were associated to typical vibrations of the  $[\text{MnO}_6]$  octahedric skeleton [37]. These bands were slightly shifted to  $705, 587, 521$  and  $463 \text{ cm}^{-1}$ , evidencing that Ru modifies the electronic environment in an indirect way. This shift has also been described previously for other isomorphic substitutions [22].

Other two appreciably less intense bands around  $3400\text{ cm}^{-1}$  and  $1600\text{ cm}^{-1}$  were also present in both materials. They were associated to water molecules adsorbed on the surface or located into the tunnel structure [33].

### UV-Vis spectroscopy

Both materials showed a common broad absorptive UV-Vis region between 300 to 600 nm (Figure S4, Supporting Information) that has been attributed to  $d - d$  transitions of manganese ions [33, 38]. [Ru]-K-OMS2 (2 wt%) showed an increase of this absorption band and a slightly blue-shifted band from 463 nm (in K-OMS2) to 445 nm for the Ru-doped sample, that suggests that ruthenium may have improved the charge transfer processes to more energetic transitions. In this regard, it is necessary to indicate that  $d - d$  transitions of manganese ions, which appear in the visible region of the spectra, have usually a moderate intensity and for that reason they are considered to be forbidden transitions [33, 38].

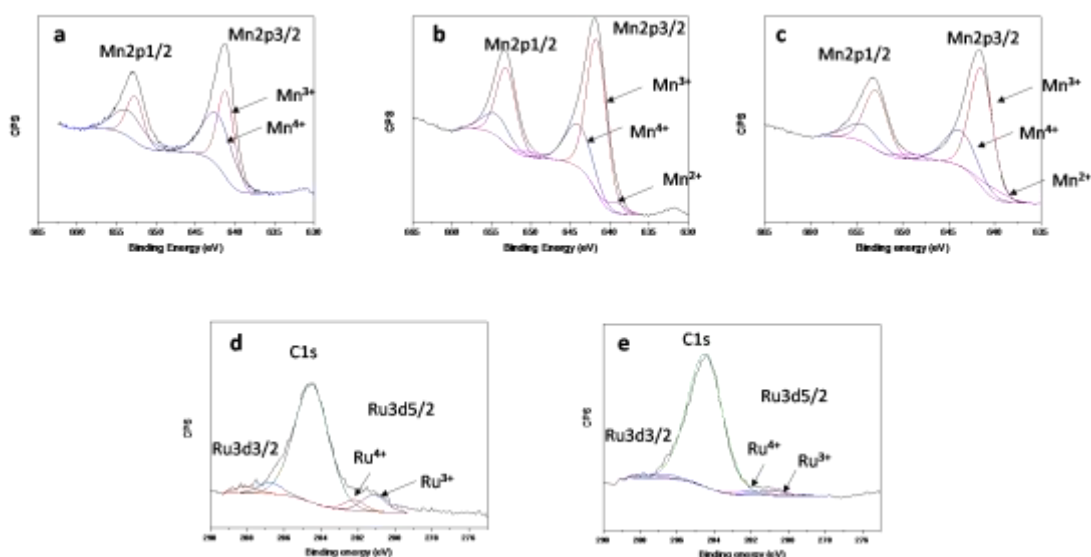
On the other hand, since the incorporation of elements into metallic oxide structures as dopants can induce variations in the band gap energy ( $E_g$ ) [38] we have estimated the band gap energy when incorporating ruthenium in [Ru]-K-OMS2 (2 wt%) following the Kubelka – Munk equation [39]. For doing that, the product of the square root of the absorption coefficient and the photon energy were plotted *versus* the incident photon energy ( $h\nu$ ). In this case a straight line in a photon energy range close to the absorption threshold was obtained giving a band gap variation from 1.31 to 1.13 for K-OMS-2 and [Ru]-K-OMS2 (2 wt%) respectively (Figure S5, Supporting Information). This experimental fact could be attributed to the introduction of new energy levels to the intra – band space by Ru ions.

It is necessary to take into account that the band gap values are strictly related not only to the nature of the elements but to synthetic factors, so that even slight variations in the synthetic procedure can give rise to different morphologies and different band gap values among the same series of manganese oxides [38, 40, 41]. At this point it can be concluded that the substitution of a fraction of Mn cations by Ru in the oxide [Ru]-K-OMS2 (2 wt%) results not only in a direct structural modification of the original K-OMS2 (i.e. size effects described in section X-Ray Diffraction and Morphology), but to a shifting of the frontier orbitals induced by the new electronic structure of the doped oxide. This fact will affect to the strength of the Mn-O bond (as discussed in section

2.4), and will also contribute to improve its properties as a semiconductor (in accordance with the new band gap values).

### XPS spectroscopy

The quantitative analysis of the oxidation states of manganese on pure K-OMS2 and Ru-doped cryptomelane [Ru]-K-OMS2 (2 wt%) was carried out by XPS analysis in the two newly prepared samples (see Figure 5).



**Figure 5:** Mn 2pXPS spectra of the fresh prepared (a) K-OMS–2 and (b) [Ru]– K-OMS2 (2 wt%) samples. (c) Mn 2p XPS spectra of [Ru]–K-OMS2 (2 wt%) after completed the reaction. Ru 3d XPS spectra of d) fresh K-OMS–2 and (e) [Ru] –K-OMS2 (2 wt%) after reaction.

These measurements confirmed the coexistence of several oxidation states for manganese in both cases, although significant differences were found at a quantitative level between both materials (Figure 5).

On one side, two different Mn 2p<sub>3/2</sub> peaks were detected at 641.3 and 642.6 eV (binding energy [BE]) that could be assigned to Mn<sup>3+</sup> and Mn<sup>4+</sup> species respectively in the K-OMS-2 sample. In this case integration of the deconvoluted peaks gave a relative abundance of 52.6% for Mn<sup>4+</sup> and 47.4% for Mn<sup>3+</sup> (Figure 5a). No other ionic Mn species were detected in the K-OMS-2 sample.

Interestingly, the XPS measurements on the Mn 2p<sub>3/2</sub> peaks of [Ru]-K-OMS2 (2 wt%) showed a remarkable decrease in the abundance of the Mn<sup>4+</sup> (26.6%) ion and an increasing of the Mn<sup>3+</sup> abundance (69.1%) together with the appearance of the more reduced Mn<sup>2+</sup> species (639.2 eV) which has an estimated abundance of *ca.* 4.3%.

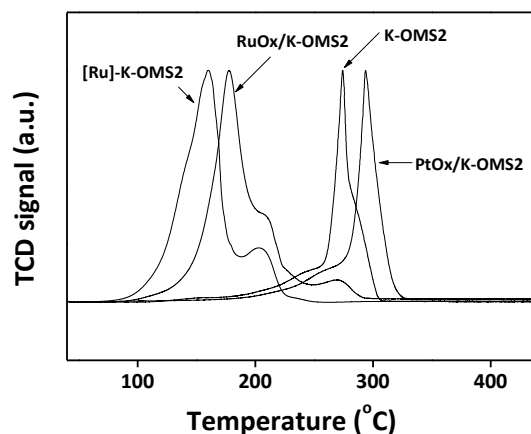
This distribution of oxidation states may not perfectly match the one obtained by ICP (see Table 1 in previous section), provided the XPS technique gives a distribution of surface oxidation states, while ICP is giving a global distribution of oxidation states (bulk).

Then, following with this XPS study, when analyzing the Ru 3d peak, two different peaks at a binding energy of 281.12 eV and 282.19 eV were associated to Ru<sup>3+</sup> and Ru<sup>4+</sup> respectively [42-45]. The Ru<sup>3+</sup>/Ru<sup>4+</sup> ratio was estimated to be *ca.* 1.86. The presence of this two oxidation states for Ru species could be explained by their combination with oxygen atoms of the surface and the lattice in agreement with TPR – H<sub>2</sub> experiments as will be shown later.

Although no others species of this element (*i.e.* Ru<sup>0</sup>) could be detected by XPS spectroscopy, we inferred that Ru<sup>3+</sup> species may be located preferably at the innermost structure given that the size and the octahedron symmetry of Ru<sup>3+</sup> is similar to Mn<sup>3+</sup> as discussed in previous section (X-Ray diffraction and morphological characterization). Moreover if we take into account that XPS data show the atomic organization on surface, in principle they do not refute the results discussed earlier in previous section (X-Ray diffraction and morphological characterization) concerning the hypothetical location of isovalent Ru<sup>3+</sup> at more internal level.

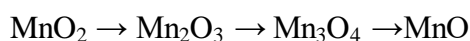
#### TPR-H<sub>2</sub> study:

In accordance with Hooke's Law which stated that the Mn-O bond has weakened by the effect of doping with Ru (see Raman and FT-IR spectroscopy section), and *a priori* this could imply a greater facility for certain redox processes, we have studied the reducibility of pure K-OMS2 as well as isomorphically substituted [Ru]-K-OMS2 (2 wt%) by H<sub>2</sub>-TPR (temperature-programmed reduction). Besides, the H<sub>2</sub>-TPR of a Ru impregnated K-OMS-2 (RuO<sub>x</sub>/K-OMS2) was also studied for comparison (Figure 6). In this case RuO<sub>x</sub>/K-OMS2 (1 wt %) was prepared by contacting K-OMS-2 with an aqueous solution containing RuCl<sub>3</sub>.xH<sub>2</sub>O under vigorous stirring, followed by filtration, drying and calcination in air (Experimental Section).



**Figure 6:** H<sub>2</sub> – TPR profiles of the materials: K-OMS-2, [Ru]-K-OMS2 (2 wt%), RuO<sub>x</sub>/K-OMS2 (1 wt%) and PtO<sub>x</sub>/K-OMS2 (1 wt%).

As can be deduced from Figure 6, the TPR profile of K-OMS2 showed a unique band around 271°C that could be decomposed into different overlapping bands and a shoulder around 245°C. All these components were assigned to the reduction of structural Mn<sup>4+</sup> and Mn<sup>3+</sup> cations involving different phase changes (*i.e.* MnO<sub>2</sub>, Mn<sub>2</sub>O<sub>3</sub>, Mn<sub>3</sub>O<sub>4</sub> and MnO), which take place following the sequence shown below [2, 36-38]:



It is important to remark that the incorporation of ruthenium into the structural lattice had a strong influence on the TPR profile of [Ru]-K-OMS2 (2 wt%) showing a remarkable displacement of the bands at lower temperatures (at 160° and 204°C) (Figure 6) [34]. It is important to indicate that the reduction of Ru<sup>4+</sup> species bound to oxygen is not detected in this case given that this process has been reported to occur at 275°C according to literature references [46,47]; while the peak at 160°C could be assigned tentatively to reduction of structural Mn cations under the influence of the dopant agent, similar to what happens with the incorporation of other elements [48-50].

In this context, it seems foreseeable that deposition of external RuO<sub>x</sub> on the K-OMS2 surface could have a less marked influence on the reducibility of the resulting material RuO<sub>x</sub>/K-OMS2 (1 wt %) than when Ru is placed at more internal positions as in fact it could be deduced from Figure 6.

Effectively, from these results it was observed that RuO<sub>x</sub>/K-OMS2 (1 wt%) experienced a less pronounced shifting of the bands at lower temperatures than [Ru]-K-OMS2 (2 wt%) (Figure 6). In line with this observation, the characteristic reduction band at 275°C that was undetectable in the Ru-doped sample [Ru]-K-OMS2 (2 wt%) was still present in the RuO<sub>x</sub>/K-OMS2 (1 wt%) sample (Figure 6). This fact is rather reasonable considering that unlike [Ru]-K-OMS2 (2 wt%), RuO<sub>x</sub>/K-OMS2 (1 wt%) presents all the ruthenium located externally on the surface.

In order to compare with other classic reducing agents, H<sub>2</sub>PtCl<sub>6</sub> · 6H<sub>2</sub>O was deposited on the surface of K-OMS-2 by a wet impregnation method, followed by filtration, drying and calcination in air (see Experimental section) and the TPR-H<sub>2</sub> profile of the resulting material (PtO<sub>x</sub>-K-OMS2 (1 wt %)) was also recorded. Interestingly, PtO<sub>x</sub>/K-OMS2 (1 wt%) presented a strong and broad H<sub>2</sub>-consumption at much higher temperature (about 300°C) [51, 52], producing just the opposite effect that Ru (Figure 6).

This result should be interpreted as PtO<sub>x</sub>/K-OMS2 (1 wt%) has a lower tendency to reduce or exchange oxygen from the surface than [Ru]-K-OMS2 (2 wt%) probably due to the presence of less reactive manganese oxide species (i.e. manganese species with a lower oxidation potential) in the Pt supported sample.

We can then say from the above results that the major effect of Ru on the cryptomelane lattice as a dopant is to weaken the Mn-O bond to ultimately increase the reducibility of the oxide; a fact that is more pronounced when Ru is forming part of the framework. This result agrees with the weakening of the Mn-O bond observed in previous Raman experiments and that will be decisive in catalysis.

### Catalytic activity

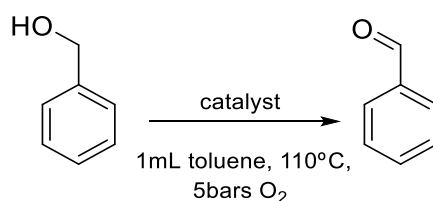
Considering that the reducibility is an essential characteristic of oxidic catalysts in oxidation reactions following a Mars van - Krevelen mechanism, and given that [Ru]-K-OMS2 (2 wt%) has shown a great capacity to remove oxygen in a relatively easy way (see Section 2), we have studied the applicability of [Ru]-K-OMS2 (2 wt%) as a catalyst for the oxidation of alcohols to aldehydes using molecular oxygen as oxidant [17-19]. To this respect it is important to indicate that the oxidation of alcohols to aldehydes has been extensively studied in the presence of manganese molecular sieves [18, 19, 53-55] as well as ruthenium catalysts although separately [56-58]. In general, stoichiometric amounts of high valent metal oxidants have been traditionally used to accomplish this



transformation, but they have high toxicity and negative economic implications [59]. For example, chromium-based reagents are toxic, irritants and corrosive; whereas manganese dioxide ( $\text{MnO}_2$ ), being more environment-friendly, has been used over the years as a highly efficient and selective catalyst for oxidation of allylic and benzylic alcohols to aldehydes, amines to imines, oxidation of CO,  $\text{H}_2\text{O}_2$  decomposition, oxygen reduction, oligomerization of methane... [19, 55, 60-64]

Table 2 includes the most important results obtained with K-OMS2, [Ru]-K-OMS2 (2 wt%) as well as other related oxides as catalysts for the selective synthesis of benzaldehyde from benzyl alcohol as model reaction.

**Table 2** Synthesis of benzaldehyde from benzyl alcohol in the presence of K-OMS2, [Ru]-K-OMS2 (2 wt%) and other related catalysts<sup>[a]</sup>.



Entry	Catalyst	Ru content (mmol%)	Conversion <sup>[b]</sup> (%)	Yield <sup>[c]</sup> (%)	Mass	
					Balance <sup>[d]</sup> (%)	TON/TOF(h <sup>-1</sup> ) <sup>[d]</sup>
<b>1</b>	<b>[Ru]-K-OMS2 (2wt%)</b>	<b>0.5</b>	<b>82</b>	<b>82</b>	<b>100</b>	<b>145/115</b>
<b>2</b>	<b>[Ru]-K-OMS2 (2wt%)</b>	<b>1.7</b>	<b>100</b>	<b>100</b>	<b>100</b>	<b>59/50</b>
3 <sup>[e]</sup>	[Ru]-K-OMS2(2wt%)	0.5	19	19	100	35/34
4	RuO <sub>x</sub> /K-OMS2 (1wt%)	0.5	61	61	100	133/82
5 <sup>[e]</sup>	RuO <sub>x</sub> /K-OMS2 (1wt%)	0.5	7	7	100	16/11
6	RuO <sub>x</sub> /K-OMS2 (2wt%)	0.8	68	68	95	88/11
7	K-OMS2	-	54	54	100	-
8 <sup>[e]</sup>	K-OMS2	-	14	14	100	-
9	MnO <sub>x</sub>	-	39	39	100	-
10 <sup>[f]</sup>	Cu/MnO <sub>x</sub> (3wt%)	-	26	26	100	54/10
11	Mn <sub>2</sub> O <sub>3</sub>	-	<2	-	99	-
12 <sup>[f]</sup>	Cu/Mn <sub>2</sub> O <sub>3</sub> (3wt%)	-	14	5.3	93	11/4
13	Mn <sub>3</sub> O <sub>4</sub>	-	0	0	100	-
14	RuO <sub>x</sub> /Al <sub>2</sub> O <sub>3</sub> (1wt%)	0.5	9	6	96	22/5
15	RuO <sub>x</sub> /ZrO <sub>2</sub> (1wt%)	0.4	17	12	95	41/30

16	RuO <sub>x</sub> /TiO <sub>2</sub> (1wt%)	0.5	15	8	94	32/22
17	---	-	-	-	100	0/0
18 <sup>g</sup>	Ag <sub>2</sub> O(1%)/MnO <sub>2</sub>	-	67	67	99	-
19 <sup>g</sup>	Ag <sub>2</sub> O(1%)/Mn <sub>2</sub> O <sub>3</sub>	-	40	40	99	-
20 <sup>h</sup>	ZrO <sub>x</sub> /Mn <sub>2</sub> O <sub>3</sub>	-	17	17	99	-

<sup>[a]</sup>Reaction conditions: 0.25 mmol benzyl alcohol, 8 – 10 mg of catalyst (~25 wt%), 1mL de toluene *n* – dodecane (internal standard), T= 110°C, P<sub>O<sub>2</sub></sub>= 5 bar, 7 hours.

<sup>[b]</sup>Conversion(%) was obtained by gas chromatography (GC) on the basis of alcohol converted.

<sup>[c]</sup>Yield (%) of benzaldehyde was obtained by GC on the basis of alcohol converted.

<sup>[d]</sup>Mass Balance (%) calculated by GC.

<sup>[d]</sup>TON: mmols of alcohol converted/mmols of doping metal; TOF: mmols of alcohol converted / mmols of doping metal x h.

<sup>[e]</sup> Reaction carried under inert atmosphere (P<sub>N<sub>2</sub></sub>= 3.5 – 4.0 bars).

<sup>[f]</sup> 1.8 mmol % Cu

<sup>[g]</sup> Reaction conditions: 2 mmol benzyl alcohol, 300mg of catalyst, O<sub>2</sub> (20ml/min), T= 100°C, 10ml toluene [65a].

<sup>[h]</sup> Reaction conditions: 2 mmol benzyl alcohol, 300mg of catalyst, O<sub>2</sub> (20ml/min), T= 100°C, 10ml toluene [65b].

As can be deduced from Table 2, cryptomelane K-OMS2, [Ru]-K-OMS2 (2 wt %) as well as the surface doped oxides RuO<sub>x</sub>/K-OMS2 (1 and 2 wt%) showed activity for the oxidation of benzyl alcohol to benzaldehyde (entries 1-2,4,6-7; Table 2) under smooth optimized conditions (see also Figure S6, Supporting Information). Moreover, they were all very selective towards obtaining benzaldehyde since in no case the presence of secondary products was detected by GC, while good mass balances were obtained in all cases (entries 1-2,4,6-7; Table 2). Among these results, [Ru]-K-OMS2 (2 wt%) gives higher activity than K-OMS2 and the two catalysts with Ru deposited on surface [RuO<sub>x</sub>/K-OMS2 (1 wt%) and RuO<sub>x</sub>/K-OMS2 (2 wt%)], which were prepared by mixing K-OMS2 with aqueous solutions containing RuCl<sub>3</sub> x H<sub>2</sub>O followed by filtration and calcination in air (see Experimental Section 6.3). Indeed, both the conversion of alcohol as well as the yield of benzaldehyde were higher according to results shown in the table (entries 1-2,4,6-7 Table 2) and Figure S6 (Supporting Information).

Even increasing the amount of isomorphically Ru-doped catalyst (up to 1.7% in Ru) it is possible to get complete conversion while maintaining excellent selectivity values and moderate TOF values (see entries 1-2, Table 2 and Figures S6 and S7, Supporting Information).

Besides, the remarkable difference of TOF values obtained with [Ru]-K-OMS2 (2 wt%) (entry 1 in Table 2; TOF: 115h<sup>-1</sup>) versus RuO<sub>x</sub>/K-OMS2 (1wt%) catalyst (entry 4 in

Table 2, TOF: 82h-1) as well as RuO<sub>x</sub>/K-OMS2 (2wt%) catalyst (entry 6 in Table 2, TOF: 11h-1) proves that the active centers produced when Ru is placed at the structural level are more reactive than when Ru is deposited at the surface level. This experimental fact is in accordance with the initial reaction rates calculated for these catalysts as shown below.

Interestingly, a control reaction in the absence of oxygen showed the existence of a residual oxidation activity by the [Ru]-K-OMS2 (2 wt%) catalyst suggesting the plausible involvement of a Mars van Krevelen mechanism, according to which the structural lattice oxygen would participate in the reaction being later reoxidized by molecular oxygen when present (entry 3, Table 2) [15, 16] as it has been already pointed out for related octahedral molecular sieves [17-19,55]. The catalytic activity of RuO<sub>x</sub>/K-OMS2 (1 wt%) and K-OMS2 was also studied under inert atmosphere just for comparison and we observed that the extension of benzylic alcohol oxidation was greater for the isomorphically substituted catalyst [Ru]-K-OMS2 (2 wt%) than for catalysts RuO<sub>x</sub>/K-OMS2 (1 wt%) and K-OMS2 (compare entries 3, 5 and 8 in Table 2). Even more, when these two kinetic reactions in the absence of oxygen were graphically represented a marked acceleration of the reaction rate was observed for the Ru-doped sample (Figure S8, Supporting Information). These results are in full agreement with the observed weakening of the Mn-O bond (see Raman and FT-IR spectroscopy section), given that if the oxygen lattice is involved in the oxidation reaction the activity of the catalyst would be inversely dependent on this Mn-O strength.

Moreover, looking carefully at the graph under inert atmosphere (Figure S8, Supporting Information), it can be deduced that in general all the Ru-doped catalysts present a higher conversion at short reaction times so that ruthenium atoms are clearly improving the mobility of the lattice oxygen along the original manganese oxide structure K-OMS2. This result can be interpreted tentatively by taking into account that formation of O-Mn-O-Ru-O groups at the surface of the oxide may cause the oxygen atoms in between Mn and Ru to be more reactive than oxygen atoms in the pure K-OMS2.

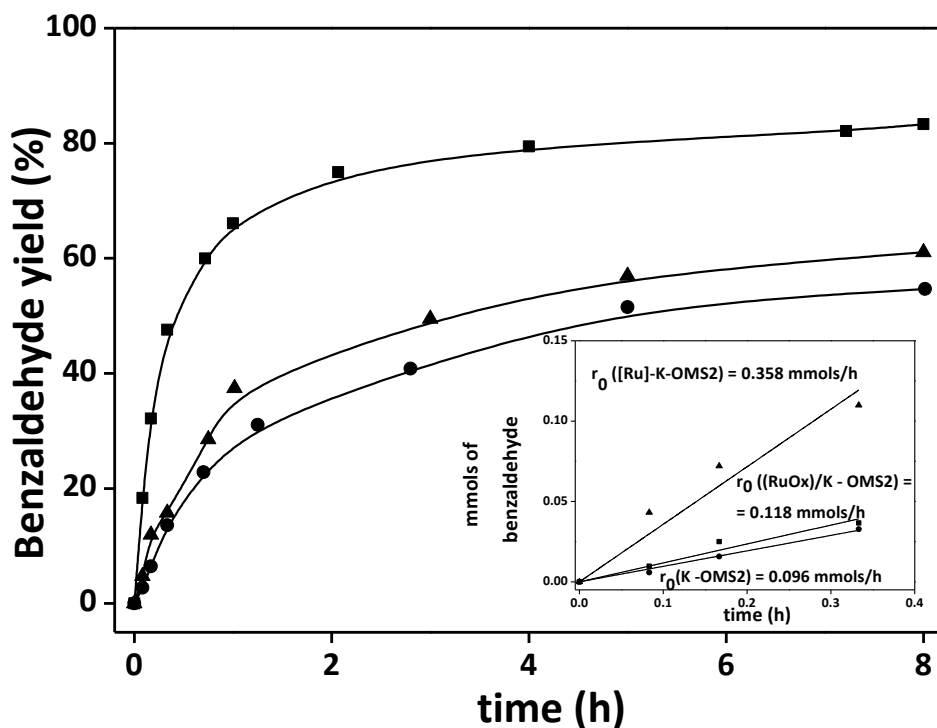
In parallel, a series of additional catalysts were tested to make a comparative study on the oxidation of benzyl alcohol to benzaldehyde. For example, different undoped and Cu-doped manganese oxides were tested as catalysts in the model reaction showing inferior catalytic results (entries 9-13, Table 2).

Besides, in order to analyze the catalytic activity of ruthenium on different supports we extended our studies to other Ru-doped catalysts using Al<sub>2</sub>O<sub>3</sub>, ZrO<sub>2</sub> and TiO<sub>2</sub> as

supports. All of these catalysts were prepared with a Ru content of 1wt % and using an impregnation method, followed by filtration and calcination in air (see Experimental section).

In this case the catalytic results included in Table 2 show that all these catalysts were inferior to [Ru]-K-OMS2 (2 wt%) confirming the importance of the pairing Ru – Mn into the structure (entries 1, 14-16). Meanwhile, no conversion was found in the absence of any catalysts (entry 17, Table 2), showing that the latter is absolutely necessary to carry out the reaction. Other related manganese oxide based catalysts doped with Ag and Zr afforded from moderate to good conversion values (entries 18-20, Table 2).[65]

In this line, Figure 7 shows the evolution of the yield of benzaldehyde with time in the presence of catalytic amounts of K-OMS2, [Ru]- K-OMS2 (2wt%) and RuO<sub>x</sub>/K-OMS2 (1wt%) materials under aerobic conditions. Initial reaction rates ( $r_0$ ) are also included in the graph for comparison.



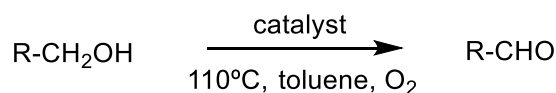
**Figure 7:** Evolution of benzaldehyde yield over time using [Ru]-K-OMS2 (2 wt%)(■), RuO<sub>x</sub>/K-OMS2 (1 wt%) (▲) and K-OMS-2 (●). The inset shows the initial reaction rate  $r_0$  calculated from the respective tangent lines for each catalyst. Reaction conditions: 0.25 mmol benzyl alcohol, 8 – 10 mg of catalyst (~25 wt%), 1mL de toluene *n* – dodecane (internal standard), T= 110°C, P<sub>O<sub>2</sub></sub>= 5 bar, 7 hours.

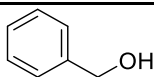
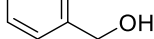
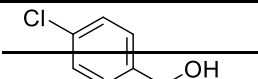
According to results included in Figure 7, the initial reaction rate for forming benzaldehyde was much higher in the presence of [Ru]-K-OMS2 (2 wt%) ( $r_0 = 0.358$  mmol/h) than the rates obtained separately with K-OMS2 ( $r_0 = 0.096$  mmol/h) or RuO<sub>x</sub>/K-OMS2 (1 wt%) ( $r_0 = 0.118$  mmol/h). Indeed, the initial reaction rate for obtaining benzaldehyde in the presence of [Ru]-K-OMS2 (2 wt%) multiplies by four the reaction rate with K-OMS-2; a fact that would be pointing to the existence of a plausible cooperative effect between manganese and ruthenium, since the impregnated RuO<sub>x</sub>/TiO<sub>2</sub> (1 wt%), RuO<sub>x</sub>(1 wt%)/Al<sub>2</sub>O<sub>3</sub> and RuO<sub>x</sub>(1 wt%)/ZrO<sub>2</sub> give noticeably lower activities (see Table 2). This interrelation between both elements may account for the observed weakening of the structural Mn-O bond as it was revealed previously (see Section 2.4).


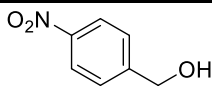
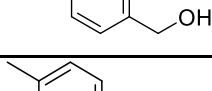
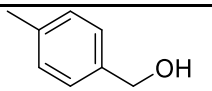
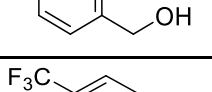
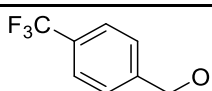
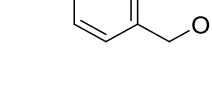
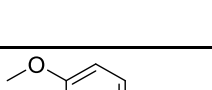
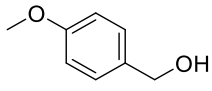
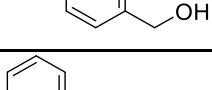
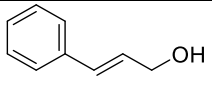
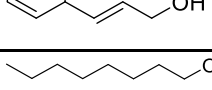
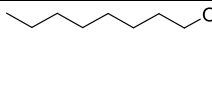
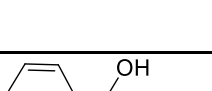
Besides, it has been confirmed that the oxidation reaction occurs on the surface of [Ru]-K-OMS2 (2 wt%), and not by dissolved Ru species, since the elimination of the solid by hot filtration at low conversion level stopped completely the reaction (Figure S9 in Supporting Information).

In parallel, the ICP analysis of the solid confirmed that the levels of Ru remain with little variation in the catalyst after four uses (see Figure S10 in Supporting Information). The scope of the reaction was studied in the presence of this catalyst [Ru]-K-OMS2 (2 wt%) and the original K-OMS-2 for comparison. The most interesting results are collected in Table 3.

**Table 3** Results on the oxidation of alcohols to aldehydes in the presence of [Ru]-K-OMS2 (2 wt%) and K-OMS-2 as catalyst<sup>[a]</sup>.



Entry	Alcohol	Catalyst	C(%) <sup>[b]</sup>	Y(%) <sup>[c]</sup>	S(%) <sup>[d]</sup>	M.B(%) <sup>[e]</sup>
1 <sup>[f]</sup>		[Ru]-KOMS2 (2 wt%)	100	100	100	100
2		[Ru]-KOMS2 (2 wt%)	82	82	100	100
3		K-OMS2	54	54	100	100
4		[Ru]-KOMS2 (2 wt%)	69	69	100	100

5		K-OMS2	36	36	100	100
6		[Ru]-KOMS2 (2 wt%)	59	59	100	96
7		K-OMS2	56	56	100	94
8		[Ru]-KOMS2 (2 wt%)	68	68	100	100
9		K-OMS2	47	47	100	98
10		[Ru]-KOMS2 (2 wt%)	61	61	100	100
11		K-OMS2	36	36	100	100
12		[Ru]-KOMS2 (2 wt%)	62	62	100	100
13		K-OMS2	43	43	100	100
14		[Ru]-KOMS2 (2 wt%)	55	55	100	100
15		K-OMS2	24	24	100	98
16		[Ru]-KOMS2 (2 wt%)	19	19	100	96
17		K-OMS2	6	<5	>99	98
18		[Ru]-KOMS2 (2 wt%)	38	38	100	96
19		K-OMS2	31	31	100	100
20 <sup>g</sup>		ZnO <sub>x</sub> (1%)/MnO <sub>2</sub>	81	81	>99	--
21 <sup>g</sup>		ZnO <sub>x</sub> (1%)/Mn <sub>2</sub> O <sub>3</sub>	56	56	>99	--

<sup>[a]</sup>Reaction conditions: 0.25 mmol benzyl alcohol, 8 – 10 mg of catalyst (~25 wt%), 1mL de toluene *n* – dodecane (internal standard), T= 110°C, P<sub>O<sub>2</sub></sub>= 5 bar, 7 hours.

<sup>[b]</sup>Conversion(%) was obtained by gas chromatography (GC) on the basis of alcohol converted.

<sup>[c]</sup>Benzaldehyde yield (%) was obtained by GC on the basis of alcohol converted.

<sup>[d]</sup> Selectivity (%) in obtaining benzaldehyde was calculated by GC.

<sup>[e]</sup> Mass Balance (%) was obtained by GC.

<sup>[f]</sup> Ru: 1.7 mmol%

<sup>[g]</sup> Reaction conditions: 2 mmol benzyl alcohol, 300mg of catalyst, O<sub>2</sub> (20ml/min), T= 100°C, 10ml toluene [66].

From the data collected in Table 3, it could be deduced that except for the reactant containing a nitro group, the incorporation of Ru has a beneficial effect on the catalytic activity during the transformation of benzyl alcohol derivatives, regardless of the electron donating or electron withdrawing nature of substituents (see entries 1-15, Table 3). Comparatively, the activity of aliphatic alcohols also experienced a clear improvement (entries 16-17, Table 3).

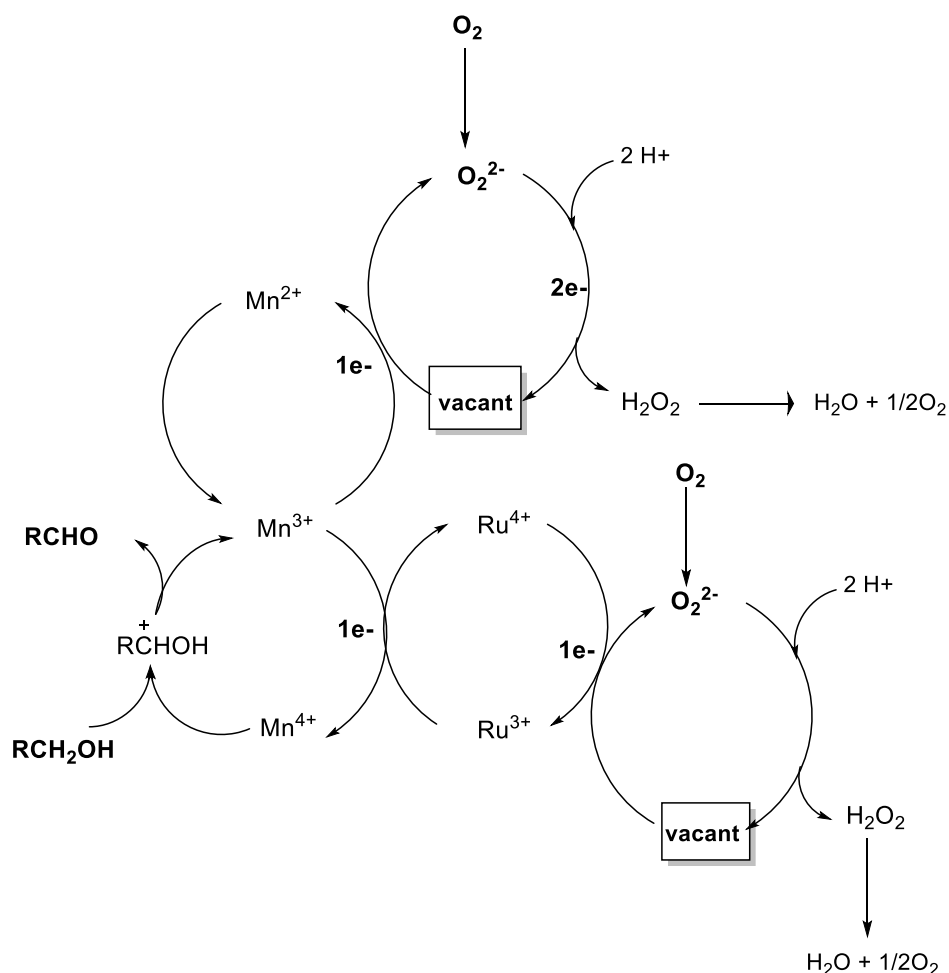
In this context, when comparing with other related manganese oxides albeit doped with Zn (i.e. ZnO<sub>x</sub> (1%)/Mn<sub>2</sub>O<sub>3</sub> and ZnO<sub>x</sub> (1%)/MnO<sub>2</sub>), it could be observed that these two Zn-doped catalysts gave better conversion values than [Ru]-KOMS2 during the

oxidation of 1-phenylethanol to acetophenone as the data included in Table 3 suggest (compare entries 18, 20-21) [66].

In summary, leaving aside previous solid monometallic Fe catalyst (prepared from a thermally pyrolyzing treatment of a Fe(III) phenantroline complex supported on graphitic oxide) [67], monometallic Au and Pd as well as bimetallic Pd/Au-based supported catalysts in the literature [68-74], the incorporation of Ru at the structural level of K-OMS2 (2 wt%) leads to a catalyst as active and selective as other known bulk Ru oxides [56] and even certain supported Ru complexes [57, 75-76]. In the next section we have attempted to understand how Ru potentiates these catalytic properties and from that, to obtain more active oxides for catalytic applications.

#### Mechanistic studies

Given that the existence of a Mars van-Krevelen mechanism would be consistent with the results obtained up to now, we speculate with the possibility that the reaction could start with the involvement of the oxygen lattice in the oxidation reaction, being the framework later reoxidized by molecular oxygen. According to this hypothesis, in a first stage the organic substrate would be oxidized and the metal would undergo a two-electron reduction from  $Mn^{4+}$  to  $Mn^{2+}$  as depicted in the following figure:



**Figure 8:** Proposed alcohol oxidation mechanism in the presence of [Ru]-K-OMS-2 (2 wt%) as a catalyst.

In a second step Mn<sup>2+</sup> would undergo a two-electron reoxidation by Ru<sup>4+</sup> which would ultimately be reoxidized by molecular oxygen (Figure 8).

In particular, the role of Ru would be restricted to reoxidize manganese reduced species to Mn<sup>3+</sup> and Mn<sup>4+</sup> and maintain the neutrality. This hypothesis seems plausible given that XPS measurements show that the manganese oxidation states practically do not vary in [Ru]-K-OMS2 (2 wt%) after use, whereas a decrease in Ru<sup>4+</sup> species and an increase in Ru<sup>3+</sup> were observed by XPS once the reaction was completed. In this regard, a limited contribution of ruthenium oxide species in the reaction cannot be discarded, as it has been previously observed with other ruthenium oxide supported catalysts (see Table 2, entries 14 – 16).



Effectively, according to XPS spectroscopy, the relative abundances of  $\text{Mn}^{2+}$ ,  $\text{Mn}^{3+}$  and  $\text{Mn}^{4+}$  ions varied from 4.3%, 69.1% and 26.6% respectively for the fresh prepared [Ru]-K-OMS-2 (2 wt%) sample, to 6.3%, 65.8% and 27.8% for  $\text{Mn}^{2+}$ ,  $\text{Mn}^{3+}$  and  $\text{Mn}^{4+}$  respectively after the reaction was completed, while the  $\text{Ru}^{3+}/\text{Ru}^{4+}$  ratio decreased from *ca.* 1.86 for the fresh prepared [Ru]-K-OMS-2 (2 wt%) to *ca.* 1.1 for the used sample.

These experimental data suggest that the catalytic activity of [Ru]-K-OMS2 (2 wt%) basically implies changes in the ionic ruthenium species content, but not for the manganese species for which these changes were not as pronounced. These results confirm that a plausible role of ruthenium would be to attend the redox pair  $\text{Mn}^{3+}/\text{Mn}^{4+}$  during the oxidation of alcohols in order to keep the electro neutrality of the structure.

In view that the participation of oxygen as electron acceptor to give water is also likely, we speculated on the possibility that the later, once formed, could ultimately poison the catalyst. At this point, the amount of water was measured by the Karl Fischer method after the reaction was completed, giving negligible moisture values for both catalysts: the Ru-doped material [Ru]-K-OMS2 (2 wt%) (<0.05 wt% water content) and K-OMS-2 (<0.04 wt% water content). [77, 78]

Given that the possibility of small amounts of water were irreversibly adsorbed on the catalyst immediately after formed cannot be completely ruled out, small amounts of water (0,6 mmol of water theoretically obtained after 40% conversion) were incorporated into the reactor before starting the reaction and the conversion of benzyl alcohol decreased moderately from 83 to 69% (Table S3, Supporting Information). This fact strongly suggests that water once formed it could adsorb on the surface of the Ru-doped material and poison the catalyst. This would also explain why water cannot be measured by the Karl-Fischer method.

In parallel, the amount of water formed on the surface of [Ru]-K-OMS2 was measured by TG analysis before and after reaction (see Section 2 and Figure S3c, Supporting Information) and as we advanced, the used catalyst [Ru]-K-OMS2 (2 wt%) experienced a greater loss of mass ( $\geq 0.47\%$  weight loss) within a low temperature range <250°C than the respective fresh catalyst. This difference in weight loss was attributed to water molecules formed on the surface of the used catalyst [Ru]-K-OMS2 (2 wt%) during the reaction.

Even more, when substoichiometric amounts of the product benzaldehyde (0.1 mmol) were incorporated into the reactor the conversion of the alcohol dropped dramatically

from 83 to 16% (Table S3, Supporting Information), hence suggesting that the adsorption of the reaction product can be the main cause of deactivation.

Finally, the possibility that some benzoic acid produced ultimately as over oxidation product was the main cause of deactivation by being strongly adsorbed on the catalyst was discarded since the incorporation of small amounts of this acid (0.1 mmol) into the reactor led to a less pronounced decrease in activity (from 83 to 50% conversion) than when adding benzaldehyde (See Table S3 in Supporting Information).

So in principle the main conclusion concerning the problem of deactivation is that the reaction product benzaldehyde strongly interacts with the catalytic centers, thereby blocking sites for the catalytic reaction [17]. Attempts were made to identify by FT-IR spectroscopy the active centers to which benzaldehyde binds. Unfortunately, the intense black color of the sample made this analysis unfeasible.

At this point studies of recovery and reuse of the catalyst were also carried out. To accomplish this, the reactor was cooled down to room temperature and degassed after the reaction was completed. The catalyst was separated by centrifugation being calcined under air at 310°C for 2 hours (heating rate = 2°C/min). The regenerated catalyst could be reused, at least, up to three times without appreciable decrease in activity and selectivity (see Supporting Information, Figure S11).

DRX studies were also carried out after use (see Supporting Information, Figure S12). Here it was observed that the crystal structure of the used [Ru]-K-OMS2 (2 wt%) was stable and did not suffer any significant variations, so that the XRD peaks and their relative intensities remained almost invariable in the diffractogram. Indeed, the XRD pattern was refined using the program FullProf and the cell parameters obtained were  $a = b = 9.8882 \text{ \AA}$  and  $c = 2.8617 \text{ \AA}$ . In this case a slight increase of the cell dimensions could be observed, a fact that is compatible with changes in the oxidation state of both elements (mainly Ru) after reaction (see section 2.6). The undoped material K-OMS2 followed the same trend after use.

Besides, the CO<sub>2</sub> surface area measurements were also performed after completing the reaction for both Ru-K-OMS2 (2wt%) and the undoped K-OMS2 material (Supporting Information, Table S2). In both cases, it was observed a decrease of the surface area value after use, which was attributed to the adsorption of organic compounds on the surface of the catalysts. Nonetheless, the area value of [Ru]-K-OMS2 (2 wt%) after use remained still above the one observed in the case of K-OMS2, evidencing again the influence of Ru.

## Conclusion

Manganese-based octahedral molecular sieve K-OMS2 was prepared by synproportionation of  $\text{KMnO}_4$  and  $\text{Mn}^{2+}$  in the presence of  $\text{Ru}^{3+}$  in acidic solution. By combining X-ray diffraction, Raman, IR, transmission and scanning electron microscopy, differential and gravimetric thermal analysis and  $\text{H}_2$ -temperature programmed it can be said that [Ru]-K-OMS2(2wt%) is a pure monophase cryptomelane material containing  $\text{Ru}^{3+}$  isomorphically incorporated into the lattice.

The most important consequence of the isomorphous substitution of Ru is the weakening of the Mn-O bond, a fact that has clear catalytic implications. It performs the oxidation of alcohols showing a complete selectivity towards the aldehyde and a clear improvement of the catalytic properties with respect the undoped catalyst due to the electronic environment modification.

The study confirms that the presence of Ru internally throughout the structure of K-OMS2 (2 wt%) has a more pronounced effect on the oxide reducibility and ultimately on the catalytic level behavior when Ru species are at or near the surface. Indeed, [Ru]-K-OMS2 (2 wt%) has shown significantly higher activity than K-OMS2 as well as the surface deposited  $\text{RuO}_x/\text{K-OMS2}$  (1wt%) and  $\text{RuO}_x/\text{K-OMS2}$  (2wt%) during the oxidation of alcohols to the corresponding aldehydes.

Leaving aside classical monometallic and bimetallic Pd and Au-based supported catalysts, the incorporation of Ru in the structure of K-OMS2 leads to a catalyst as active and selective as bulk Ru oxides or even Ru supported complexes.

The heterogeneity of the process has been confirmed and the catalyst has been recovered and reused without a significant loss of activity and catalytic properties. Besides, the regeneration of deactivated [Ru]-K-OMS2 (2 wt%) can be achieved by calcination in air.

## Experimental

### Materials:

Potassium permanganate ( $\geq 99.9\%$ ,  $\text{KMnO}_4$ ), manganese sulfate monohydrate ( $\geq 99.9\%$ ,  $\text{MnSO}_4 \cdot \text{H}_2\text{O}$ ) and ruthenium(III) chloride hydrate (39.96%,  $\text{RuCl}_3 \cdot x\text{H}_2\text{O}$ ) were supplied

by Sigma–Aldrich (Merck), Probus S.A. and Johnson Mathey, respectively. Nitric acid 65% technical grade was purchased from Panreac. All chemicals were used as received without further purification.

Synthesis of the [Ru] – K – OMS2 catalyst:

The synthesis has been carried out following the basis procedure described in the literature with modifications [10] :

Synthesis of [Ru]-K-OMS2 (2 wt %): 2.29g of potassium permanganate (0.014mols) in 40mL of Milli – Q was added to a solution of 3.52g of manganese sulphate monohydrate (0.021 mols) in 12mL of Milli – Q water and 1.2mL nitric acid (65%). Then, 0.242g of ruthenium(III) chloride hydrate (0.018M reaction solution) was added to the solution. The solution was refluxed at 100°C for 24h. The final solution was centrifuged to remove the solvent and the solid was washed with water until neutral pH, being dried at 100°C overnight. A black solid was obtained.

Synthesis of K - OMS2, Mn<sub>2</sub>O<sub>3</sub>, MnO<sub>x</sub>, Cu(3%)/ Mn<sub>2</sub>O<sub>3</sub>, Cu(3%)/MnO<sub>x</sub> catalyst:

The synthesis of the undoped material K-OMS2 was carried out following a known experimental procedure [79-80]. The synthesis of the oxides Mn<sub>2</sub>O<sub>3</sub> and MnO<sub>x</sub> as well as the respective doped materials (Cu(3%)/ Mn<sub>2</sub>O<sub>3</sub> and (Cu(3%)/ MnO<sub>x</sub> following a reported procedure[52].

Synthesis of the RuO<sub>x</sub>/K-OMS2 catalyst:

a) RuO<sub>x</sub>/K-OMS2 (1 wt%): The synthesis of supported ruthenium oxide on the manganese oxide (RuO<sub>x</sub>/K-OMS2) is based on an impregnation method from a ruthenium salt precursor. 8.76mg of RuCl<sub>3</sub>·nH<sub>2</sub>O were dissolved in 25mL MilliQ water and, under vigorous stirring, 350 mg of OMS2 was added. The stirring was maintained for overnight. The suspension was filtered and washed several times with MilliQ water until neutral pH. The solid was dried at 100°C for 8 hours. A black – brown solid was obtained. Before using in reaction, the catalyst was calcined under air at 500°C for 6 hours (heating rate = 2°C/min) in order to obtain the oxide of ruthenium, as it has been previously described in the literature[24].

a) RuO<sub>x</sub>/K-OMS2 (2 wt%) : The synthesis of supported ruthenium oxide on the manganese oxide (RuO<sub>x</sub>/K-OMS2) is based on an impregnation method from a ruthenium salt precursor. 17,52 mg of RuCl<sub>3</sub>·nH<sub>2</sub>O were dissolved in 25mL MilliQ

water and, under vigorous stirring, 350 mg of OMS2 was added. The stirring was maintained for overnight. The suspension was filtered and washed several times with MilliQ water until neutral pH. The solid was dried at 100°C for 8 hours. A black – brown solid was obtained. Before using in reaction, the catalyst was calcined under air at 500°C for 6 hours (heating rate = 2°C/min) in order to obtain the oxide of ruthenium, as it has been previously described in the literature[24].

#### Synthesis of other RuO<sub>x</sub> supported catalysts:

The synthesis of supported ruthenium oxides (RuO<sub>x</sub>/Al<sub>2</sub>O<sub>3</sub>, RuO<sub>x</sub>/TiO<sub>2</sub>, RuO<sub>x</sub>/ZrO<sub>2</sub>) was carried out by following a classic impregnation method [81]. The appropriate amount of RuCl<sub>3</sub>·nH<sub>2</sub>O was dissolved in 30mL MilliQ water and the necessary amount of support were added being mixed stirred under vigorous stirring (Al<sub>2</sub>O<sub>3</sub>, TiO<sub>2</sub>, ZrO<sub>2</sub>). The suspensions were filtered being washed exhaustively with MilliQ water until neutral pH. The solids were dried at 100°C for 8 hours. Then the resulting catalysts were calcined under air at 500°C for 6 hours (heating rate = 2°C/min).

#### Synthesis of PtO<sub>x</sub>/K-OMS2 (1 wt %):

The synthesis of platinum oxide supported on the manganese oxide (PtO<sub>x</sub>/K-OMS – 2) was carried out by following a classic impregnation method. In this case, 6.6mg of H<sub>2</sub>PtCl<sub>6</sub>·6H<sub>2</sub>O were dissolved in 25mL MilliQ water and 249 mg of K-OMS2 were added under vigorous stirring. The resulting slurry was left stirring overnight. The suspension was filtered and washed several times with MilliQ water until neutral pH. The solid was dried at 100°C for 8 hours. The catalyst was calcined under air at 400°C for 4 hours (heating rate = 2°C/min) [51]

#### Catalytic studies:

The catalytic reactions were carried out at 110°C and 5 bar O<sub>2</sub> using a reactor equipped with a manometer and a microsampling system which allowed the extraction of reaction samples at regular reaction times. Under typical reaction conditions 0.25 mmol benzyl alcohol, 1mL toluene and the proper amount of catalyst were charged into the reactor, which was purged with oxygen up to 10 times being pressurized at 5 bar. The reaction was monitored by gas chromatography using an HP-5 capillary column (5% phenylmethylsiloxane, 30 m x 320µm x 0.25µm). Products were identified by GC – MS

using an Agilent 6890N8000 equipped with a mass spectrometry detector (Agilent 5973N quadrupole detector).

#### Recovery and reuse studies

Once the reaction was completed, the reactor was cooled down to room temperature and degassed. The catalyst was separated by centrifugation. Before each reuse, the catalyst was calcined under air at 310°C for 2 hours (heating rate = 2°C/min). The regenerated catalyst was introduced back into the reactor and new amounts of benzyl alcohol and internal standard were added. The system was pressurized with oxygen (5 bar) and the reactor was brought to 110°C. The reaction was again monitored by gas chromatography at certain time intervals.

#### Leaching experiments

They were carried out by removing the catalyst from the reaction mixture at certain reaction time (filtration) and monitoring the activity of the liquid by GC.

### **Analyses and Instrumentation**

#### a) Inductively Coupled Plasma-Atomic Emission Spectroscopy (ICP-AES) Analysis:

The chemical compositions were measured by Inductively Coupled Plasma-Atomic Emission Spectroscopy (ICP-AES) analysis. The chemical analyses were carried out in a Varian 715-ES ICP Optical Emission spectrometer, after the solid was dissolved in HNO<sub>3</sub>/HCl (1:3) + H<sub>2</sub>O<sub>2</sub>/H<sub>2</sub>SO<sub>4</sub> aqueous solution.

b) X-ray Diffraction (XRD): The crystal structure of the as-prepared samples was verified by X-ray powder diffraction. X-ray powder diffraction (XRPD) data of the cryptomelane samples, both undoped and Ru-doped, were collected using a PANalytical CUBIX X-ray diffractometer with Cu K $\alpha$  radiation and fixed divergence slits in the 2 $\theta$  range from 10 to 100°.

c) Temperature Programmed Reduction (TPR): H<sub>2</sub>-TPR (temperature programmed reduction) profiles were obtained using Autochem 2910 with a thermal conductivity detector (TCD). Among forty – fifty milligrams of solid (granulometry: 0.4 – 0.8mm) was placed in a quartz tube, heated to 105 °C and purged with argon gas (Ar) for 30

minutes, and then reduced in a stream of a mixture of 10% H<sub>2</sub>/Ar (50.01 mL/min) at a heating rate of 5 °C/min to 600 °C.

d) X-ray Photoelectron Spectroscopy (XPS): The surface composition and the chemical state of ruthenium and manganese were determined by X-ray Photoelectron Spectroscopy (XPS). Photoelectron spectra were recorded using a SPECS spectrometer equipped with a 150MCD (Magnetic Circular Dichroism) – 9 Phoibos detector and using a monochromatic Mg K $\alpha$  (1253.6eV) X – ray source for the undoped material and a non – monochromatic Al K $\alpha$  (1486.6eV) X – ray source for the doped material. Spectra were recorded using an analyzer pass energy of 30 eV, an X – ray power of 100W and under an operating pressure of 10<sup>-9</sup>mbar.

During data processing, binding energy (BE) values were referenced to C1s peak (284.5 eV). Spectra treatment has been performed using the CASA software.

e) Raman and FT-IR spectroscopy: Solid IR (Infrared) spectra of the undoped and doped materials were recorded on a Thermo Nicolet iS10 spectrophotometer by previous mixture with KBr. Raman measurements were taken at room temperature with a 785nm laser excitation on a Renishaw Raman Sepectrometer (“in via”) equipped with a CCD detector. The spectrometer was calibrated with a silicon wafer before each Raman measurement.

f) UV-Vis spectroscopy: UV – visible absorption data were collected on Cary 50 Bio UV – visible spectrophotometer. Quartz cells of 1 cm optical path length were employed for all measurements. Samples were prepared by ultrasonically dispersing an amount of the desired solid in MilliQ water. After that, an aliquot of this suspension is taken and it was diluted in MilliQ water in order to get a concentration of 0.19 g/L or 0.06 g/L.

g) TEM and SEM Microscopy: The morphology of the samples was studied using a JEOL 2100F microscope operating at 200kV both in transmission (TEM) and scanning – transmission mode (STEM). STEM images were obtained using a High Angle Annular Dark Field detector (HAADF), which allows Z-contrast imaging. Samples were prepared by dropping the suspension of OMS2 and [Ru] – OMS2 using CH<sub>2</sub>Cl<sub>2</sub> as the solvent directly onto holey-carbon-coated nickel grids.

SEM images were recorded with a ZEISS Ultra-55 and a ZEISS Auriga – Compact field- emission scanning electron microscope operating at an accelerating voltage of

2kV. XEDS was performed with an Oxford LINK ISIS system connected to a JEOL 6300 electron microscope with the SEMQUANT program, which introduces ZAF correction. The counting time for each analysis was 100 s. Also XEDS was performed connected to a JEOL JEOL 2100F and using the same software. The solid powder sample was adsorbed on conductive carbon tape.

h) Thermogravimetric studies: Thermogravimetric analyses (TGA and DTG) were conducted in a nitrogen stream with a NETZSCH STA 449 F3 Jupiter analyzer. The range of temperature was 25°C to 700°C with a heating rate of 10K/min. Any specific pre-treatment has been done before the measure.

i) CO<sub>2</sub> surface area measurements:

Dioxide carbon physisorption experiments were done at 273 K using an ASAP 2010 physisorption apparatus. The Dubinin-Radushkevich equation was used to fitting the isotherms.

### **Acknowledgements:**

Financial support by the Ministerio de Economía y Competitividad, Programa Severo Ochoa (SEV2016-0683) and Ministerio de Ciencia Innovación y Universidades, Programa Estatal de Generación de Conocimiento (PGC2018-101247-B-100) are gratefully acknowledged.

F.S. thanks to Ministerio de Ciencia, Innovación y Universidades for the economic support (Ayuda Predoctoral FPI – Severo Ochoa).

The Electron Microscope of the Universitat Politècnica de València is acknowledged for their help in the characterization of samples.

### **Conflicts of interest**

There are no conflicts to declare.

### **References:**

- [1] H. Chen, Y. Wang, Y.-K. Lv, *RSC Advances*, 2016, **6**, 54032-54040.
- [2] S. L. Suib, Sorption, catalysis and separation design, *Chemical Innovation*, 2000, 30(3), 27-33.
- [3] T.T. Truong, Y. Liu, Y. Ren, L. Trahey, Y. Sun, *ACS Nano*, 2012, **6**, 8067-8077.



- [4] M. Huang, Y. Zhang, F. Li, L. Zhang, R.S. Ruoff, Z. Wen, Q. Liu, *Scientific Reports*, 2014, **4**, 3878.
- [5] O. Ghodbane, J.-L. Pascal, B. Fraisse, F. Favier, *ACS Applied Materials & Interfaces*, 2010, **2**, 3493-3505.
- [6] *New and Future Developments in Catalysis*, S.L. Suib (Ed.), Elsevier, Amsterdam, 2013; ISBN: 9780444538826.
- [7] N. Subramanian, B. Viswanathan, T.K. Varadarajan, *RSC Advances*, 2014, **4**, 33911-33922.
- [8] M.A. Peluso, L.A. Gambaro, E. Pronso, D. Gazzoli, H.J. Thomas, J.E. Sambeth, *Catalysis Today*, 2008, **133-135**, 487-492.
- [9] H. Yin, X. Dai, M. Zhu, F. Li, X. Feng, F. Liu, *Journal of Hazardous Materials*, 2015, **296**, 221-229.
- [10] C.K. King'ondo, N. Opembe, C.h. Chen, K. Ngala, H. Huang, A. Iyer, H.F. Garcés, S.L. Suib, *Advanced Functional Materials*, 2011, **21**, 312-323.
- [11] R.N. DeGuzman, Y.-F. Shen, E.J. Neth, S.L. Suib, C.-L. O'Young, S. Levine, J.M. Newsam, , *Chemistry of Materials*, 1994, **6**, 815-821.
- [12] Y.-s. Ding, X.-f. Shen, S. Sithambaram, S. Gomez, R. Kumar, V.M.B. Crisostomo, S.L. Suib, M. Aindow, *Chemistry of Materials*, 2005, **17**, 5382-5389.
- [13] L. Liu, H. Zhao, J.M. Andino, Y. Li, *ACS Catalysis*, 2012, **2**, 1817-1828.
- [14] Aldehydes and Ketones, *Hamilton & Hardy's Industrial Toxicology*, R. D. Harbison, M. M. Bourgeois, G.T. Johnson (Eds), 2015, John Wiley and Sons Inc., ISBN: 9780470929735.
- [15] Y. Moro-oka, W. Ueda, K.-H. Lee, *Journal of Molecular Catalysis A: Chemical*, 2003, **199**, 139-148.
- [16] P. Mars, D.W. van Krevelen, *Chemical Engineering Science*, 1954, **3**, 41-59.
- [17] F. Schurz, J.M. Bauchert, T. Merker, T. Schleid, H. Hasse, R. Gläser, *Applied Catalysis A: General*, 2009, **355**, 42-49.
- [18] V.D. Makwana, Y.-C. Son, A.R. Howell, S.L. Suib, *Journal of Catalysis*, 2002, **210**, 46-52.
- [19] V.D. Makwana, L.J. Garces, J. Liu, J. Cai, Y.-C. Son, S.L. Suib, *Catalysis Today*, 2003, **85**, 225-233.
- [20] J. Vicat, E. Fanchon, P. Strobel, D. Tran Qui, *Acta Crystallographica Section B*, 1986, **42**, 162-167.

- [21] J. Carvajal, FULLPROF: A Program for Rietveld Refinement and Pattern Matching Analysis, *Abstracts of the Satellite Meeting on Powder Diffraction of the XV Congress of the IUCr*, (1990).
- [22] L.R. Pahalagedara, S. Dharmarathna, C.K. King'onde, M.N. Pahalagedara, Y.T. Meng, C.H. Kuo, S.L. Suib, *The Journal of Physical Chemistry C*, 2014, **118**, 20363-20373.
- [23] G.H.Genuino, Y. Meng, D. T. Horvath, C-H. Kuo, M.S. Seraji, A. M. Morey, R. L. Joesten, S.L. Suib., *ChemCatChem*, 2013, **5**, 2306-2317.
- [24] M. Polverejan, J.C. Villegas, S.L. Suib, *Journal of the American Chemical Society*, 2004, **126**, 7774-7775.
- [25] L. Pauling, *The Nature of the Chemical Bond*, 3<sup>rd</sup>ed., Cornell University Press, Ithaca, United States, 1960.
- [26] L.H. Ahrens, *Geochimica et Cosmochimica Acta*, 1952, **2**, 155-169.
- [27] Q. Feng, H. Kanoh, Y. Miyai, K. Ooi, *Chemistry of Materials*, 1995, **7**, 148-153.
- [28] C. Calvert, R. Joesten, K. Ngala, J. Villegas, *Chemistry of Materials*, 2008, **20**, 6382-6388.
- [29] J. Luo, Q. Zhang, J. Garcia-Martinez, S.L. Suib, *Journal of the American Chemical Society*, 2008, **130**, 3198-3207.
- [30] X. Wu, X. Yu, Z. Chen, Z. Huang, G. Jing, *Catalysis Science & Technology*, 2019, **9**, 4108-4117.
- [31] A.M. El-Sawy, C.K. King'onde, C.-H. Kuo, D.A. Kriz, C.J. Guild, Y. Meng, S.J. Frueh, S. Dharmarathna, S.N. Ehrlich, S.L. Suib, *Chemistry of Materials*, 2014, **26**, 5752-5760.
- [32] X. Li, J. Ma, X. Jia, F. Xia, Y. Huang, Y. Xu, J. Xu, *ACS Sustainable Chemistry & Engineering*, 2018, **6**, 8048-8054.
- [33] T. Gao, M. Glerup, F. Krumeich, R. Nesper, H. Fjellvåg, P. Norby, *The Journal of Physical Chemistry C*, 2008, **112**, 13134-13140.
- [34] S. Sultana, Z. Ye, S.K.P. Veerapandian, A. Löfberg, N. De Geyter, R. Morent, J.-M. Giraudon, J.-F. Lamonier, *Catalysis Today*, 2018, **307**, 20-28.
- [35] K.A. V., H. Ying-Sheng, T. Kwong-Kau, T. Dah-Shyang, *Journal of Raman Spectroscopy*, 2007, **38**, 737-749.
- [36] J. Hou, Y. Li, L. Liu, L. Ren, X. Zhao, *Journal of Materials Chemistry A*, 2013, **1**, 6736-6741.

- [37] M. Ousmane, G. Perrussel, Z. Yan, J.M. Clacens, F. De Campo, M. Pera-Titus, *Journal of Catalysis*, 2014, **309**, 439-452.
- [38] W. Li, X. Cui, R. Zeng, G. Du, Z. Sun, R. Zheng, S.P. Ringer, S.X. Dou, *Scientific Reports*, 2015, **5**, 8987.
- [39] P. Kubelka, F. Munk, *Zeitschrift für Technische Physik*, 1931, **12**, 593-601.
- [40] C. Lume-Pereira, S. Baral, A. Henglein, E. Janata, *The Journal of Physical Chemistry*, 1985, **89**, 5772-5778.
- [41] N. Sakai, Y. Ebina, K. Takada, T. Sasaki, *The Journal of Physical Chemistry B*, 2005, **109**, 9651-9655.
- [42] D.J. Morgan, *Surface and Interface Analysis*, 2015, **47**, 1072-1079.
- [43] W. Wang, S. Guo, I. Lee, K. Ahmed, J. Zhong, Z. Favors, F. Zaera, M. Ozkan, C.S. Ozkan, , *Scientific Reports*, 2014, **4**, 4452.
- [44] K.C. Park, I.Y. Jang, W. Wongwiryapan, S. Morimoto, Y.J. Kim, Y.C. Jung, T. Toya, M. Endo, *Journal of Materials Chemistry*, 2010, **20**, 5345-5354.
- [45] Y. Park, B. Lee, C. Kim, Y. Oh, S. Nam, B. Park, *Journal of Materials Research*, 2011, **24**, 2762-2766.
- [46] H. Zhang, W. Li, Y. Jin, W. Sheng, M. Hu, X. Wang, J. Zhang, *Applied Catalysis B: Environmental*, 2016, **189**, 56-64.
- [47] B. Man, H. Zhang, J. Zhang, X. Li, N. Xu, H. Dai, M. Zhu, B. Dai, *RSC Advances*, 2017, **7** 23742-23750.
- [48] W.Y. Hernández, M.A. Centeno, S. Ivanova, P. Eloy, E.M. Gaigneaux, J.A. Odriozola, *Applied Catalysis B: Environmental*, 2012, **123-124**, 27-35.
- [49] A. Davó-Quiñonero, M. Navlani-García, D. Lozano-Castelló, A. Bueno-López, *Catalysis Science & Technology*, 2016, **6**, 5684-5692.
- [50] F. Sabaté, J. Navas, M.J. Sabater, A. Corma, *Comptes Rendus Chimie*, 2018, **21**, 164-173.
- [51] R. Wang, J. Li, *Catalysis Letters*, 2009, **131**, 500-505.
- [52] C. Zhang, H. He, K.-i. Tanaka, *Applied Catalysis B: Environmental*, 2006, **65**, 37-43.
- [53] J.R. Kona, C. K. King'andu, A.R. Howell, S. L. Suib, *ChemCatChem*, 2014, **6**, 749-752.
- [54] N.N. Opembe, C. Guild, C. King'andu, N.C. Nelson, I.I. Slowing, S.L. Suib, *Industrial & Engineering Chemistry Research*, 2014, **53**, 19044-19051.

- [55] A. Doménech-Carbó, F. Sabaté, M.J. Sabater, *The Journal of Physical Chemistry C*, 2018, **122**, 10939-10947.
- [56] A. Köckritz, M. Sebek, A. Dittmar, J. Radnik, A. Brückner, U. Bentrup, M.M. Pohl, H. Hugl, W. Mägerlein, *Journal of Molecular Catalysis A: Chemical*, 2006, **246**, 85-99.
- [57] K.J. Won, K. Takeshi, K. Miyuki, Y. Kazuya, M. Noritaka, *Chemistry – A European Journal*, 2008, **14**, 4104-4109.
- [58] G. Liu, J. Liu, W. Li, C. Liu, F. Wang, J. He, C. Guild, J. Jin, D. Kriz, R. Miao, S.L. Suib, *Applied Catalysis A: General*, 2017, **535**, 77-84.
- [59] A. Chakravarty, D. Sengupta, B. Basu, A. Mukherjee, G. De, *RSC Advances*, 2015, **5**, 92585-92595.
- [60] S. Cheng, X. Ma, Y. Hu, B. Li, *Applied Organometallic Chemistry*, 2017, **31**, e3659.
- [61] J.-H. Park, D.-C. Kang, S.-J. Park, C.-H. Shin, *Journal of Industrial and Engineering Chemistry*, 2015, **25**, 250-257.
- [62] C. Fan, A. Lu, Y. Li, C. Wang, *Journal of Colloid and Interface Science*, 2008, **327**, 393-402.
- [63] Y. Yang, X. Su, L. Zhang, P. Kerns, L. Achola, V. Hayes, R. Quardokus, S.L. Suib, J. He, *ChemCatChem*, 2019, **11**, 1689-1700.
- [64] C. Marún, L.D. Conde, S.L. Suib, *The Journal of Physical Chemistry A*, 1999, **103**, 4332-4340.
- [65] a) M.E. Assal, M. R. Shaik, M. Kuniyil, M. Khan, A. Al-Warthan, A. I. Alharthi, R. Varala, M. R. H. Siddiqui, S. F. Adil, *Arab. J. Chem.*, 2019, **12**, 54-68; b) M.E. Assal, M. R. Shaik, M. Kuniyil, M. Khan, A. Al-Warthan, M.R.H. Siddiqui, S.M.A. Khan, W. Tremel, M. N. Tahir, S. F. Adil, *RSC Advances*, 2017, **7**, 55336 -55349.
- [66] M.E. Assal, M. Kuniyil, M. R. Shaik, M. Khan, A. Al-Warthan, M.R.H. Siddiqui, S. F. Adil, *J. Chem.*, 2017, <https://doi.org/10.1155/2017/2937108>
- [67] a) G. Jaiswal, V. G. Landge, D. Jagadeesan, E. Balaraman, *Nat. Commun.*, 2017, **8**, 2147, doi:10.1038/s41467-017-01603-3; b) C. Gunanathan, D. Milstein, *Chem. Rev.*, 2014, **114**, 12024-12087.
- [68] J. Chen, Q. Zhang, Y. Wang, H. Wan, *Advanced Synthesis & Catalysis*, 2008, **350**, 453-464.
- [69] K. Layek, H. Maheswaran, R. Arundhathi, M.L. Kantam, S.K. Bhargava, *Advanced Synthesis & Catalysis*, 2011, **353**, 606-616.

- [70] A. Savara, C.E. Chan-Thaw, I. Rossetti, A. Villa, L. Prati, *ChemCatChem*, 2014, **6**, 3464-3473.
- [71] T. Mitsudome, A. Noujima, T. Mizugaki, K. Jitsukawa, K. Kaneda, *Advanced Synthesis & Catalysis*, 2009, **351**, 1890-1896.
- [72] O. Casanova, S. Iborra, A. Corma, *ChemSusChem*, 2009, **2**, 1138-1144.
- [73] M. Boronat, A. Corma, F. Illas, J. Radilla, T. Ródenas, M.J. Sabater, *Journal of Catalysis*, 2011, **278**, 50-58.
- [74] A. Abad, A. Corma, H. García, *Chemistry – A European Journal*, 2008, **14**, 212-222.
- [75] K. Yamaguchi, N. Mizuno, Supported Ruthenium Catalyst for the Heterogeneous Oxidation of Alcohols with Molecular Oxygen, *Angewandte Chemie International Edition*, 2002, **41**, 4538-4542.
- [76] K. Yamaguchi, N. Mizuno, *Chemistry – A European Journal*, 2003, **9**, 4353-4361.
- [77] E.D. Peters, J.L. Jungnickel, *Analytical Chemistry*, 1955, **27**, 450-453.
- [78] M. Margreth, R. Schlink, A. Steinbach, *Water Determination By Karl Fischer Titration*, Analysis and Pharmaceutical Quality, Wiley Online Library, 2010.
- [79] Y.C. Son, V. D. Makwana, A. R. Howell, S. L. Suib, *Angewandte Chemie International Edition*, 2001, **40**, 4280-4283.
- [80] S. Ching, K.S. Krukowska, S.L. Suib, *Inorganica Chimica Acta*, 1999, **294**, 123-132.
- [81] P. Betancourt, A. Rives, R. Hubaut, C.E. Scott, J. Goldwasser, *Applied Catalysis A: General*, 1998, **170**, 307-314.